Local Electronic Structure near Mn Acceptors in InAs: Surface-Induced Symmetry Breaking and Coupling to Host States

F. Marczinowski,[1] J. Wiebe,[1,*] J.-M. Tang,[2,†] M. E. Flatté,[2] F. Meier,[1] M. Morgenstern,[3] and R. Wiesendanger[1]

[1]*Institute of Applied Physics, Hamburg University, Jungiusstrasse 11, D-20355 Hamburg, Germany*[‡]

[2]*Optical Science and Technology Center and Department of Physics and Astronomy, University of Iowa, Iowa City, Iowa 52242, USA*

[3]*II. Institute of Physics B, RWTH Aachen University, Physikzentrum Melaten, Otto-Blumenthal-Strasse, D-52056 Aachen, Germany*

(Received 25 April 2007; published 9 October 2007)

We present low-temperature scanning tunneling spectroscopy measurements on Mn acceptors in InAs in comparison with tight-binding calculations. We find a strong (001)-mirror asymmetry of the bound hole wave function close to the (110) surface. In addition, multiple acceptor-related peaks are observed and are attributed to a spin-orbit splitting of the acceptor level. Because of the *p-d* exchange interaction the local density of states near the acceptors is enhanced in the valence band and suppressed in the conduction band. We also observe signs of anisotropic scattering of the conduction band states by neutral acceptors.

DOI: 10.1103/PhysRevLett.99.157202 PACS numbers: 75.50.Pp, 72.10.Fk, 73.61.Ey, 75.30.Hx

Diluted magnetic semiconductors show promise for seamless integration of magnetic elements in electronic devices [1–4]. However, the ongoing search for room-temperature ferromagnetism in semiconductors, a prerequisite for the realization of many of the proposed devices, calls for a detailed investigation of the local coupling between the magnetic impurities and the host material. An excellent tool for such local investigations is scanning tunneling microscopy (STM), which provides unrivaled spatial resolution [5]. Recent STM measurements revealed that the hole state bound to a Mn acceptor in GaAs [6] and InAs [7] has an anisotropic crosslike shape which persists up to short Mn-Mn distances [8]. This implies a strong influence of the shape anisotropy on the local coupling and, indeed, an anisotropic exchange interaction between neighboring Mn atoms has been observed by STM at the GaAs(110) surface [9]. The STM observations so far are in agreement with theoretical predictions [10,11]. However, the detailed influence of the Mn acceptor on the local density of states (LDOS) in the host bands, and the effect of an interface on the bound states themselves, have not been elucidated so far. The Mn acceptor state in InAs provides an opportunity for all these investigations, with well-characterized surface properties and a Mn binding energy of $E_B = 28$ meV (about one quarter the binding energy in GaAs due to a weaker *p-d* exchange interaction, but still about twice the hydrogenic binding energy, 17 meV [12–14]). We show that the (110) surface leads to a substantial increase in the asymmetry of the bound hole state. Moreover, detailed spectroscopic data exhibit excited states of the acceptor, an enhancement of the valence band (VB) LDOS and reduction of the conduction band (CB) LDOS in a region of 2 nm around the acceptor, and an anisotropic shape of the scattering states in the CB. Most of the results are in accordance with tight-binding model (TBM) calculations, showing the importance of local anisotropies principally caused by the *p-d* exchange interaction.

The measurements are performed in two different low-temperature ultrahigh vacuum STM facilities with $T \approx 4$ K using electrochemically etched polycrystalline tungsten tips flashed *in situ* to $T = 2300$ K [15,16]. The Mn concentration within the InAs samples is $\sim 1 \times 10^{19}$ cm^{-3} and the samples show paramagnetic behavior down to $T = 2$ K. The clean (110) surface is prepared by *in situ* cleavage [17]. STM topographs showing the position and the shape of the Mn acceptors are taken in constant current mode with the voltage V applied to the sample. The differential conductance $dI/dV(\mathbf{r}, V)$ as a function of position $\mathbf{r}$ and bias voltage V is taken by lock-in technique using a modulation voltage V_{mod}. A stabilization voltage V_{stab} and current I_{stab} is used to stabilize the tip-surface distance at each position $\mathbf{r}$. $dI/dV(\mathbf{r}, V)$ is a measure for the LDOS [5].

For the TBM calculations, we use the theory of Ref. [10], a Koster-Slater approach with a 16-band sp^3 TBM for InAs [18]. Most of the state's binding energy comes from the *p-d* exchange interaction, which is modeled as a spin-dependent potential (V_{pd}) present at the four 1st-nearest-neighbor sites. $V_{\mathrm{pd}} = 2.19$ eV is set to obtain the experimental binding energy E_B. This value is smaller than the 3.634 eV previously obtained for GaAs [19]. An on-site potential (V_n) accounts for the direct Coulomb contribution to the binding energy, and is chosen to be the same value as for Mn in GaAs (1 eV). Thus,

$$V_{\mathrm{Mn}} = V_n \sum_{\ell,s} c^{\dagger}_{0,\ell,s} c_{0,\ell,s} + V_{\mathrm{pd}} \sum_{j \in 1^{\mathrm{st}}\mathrm{NN}, \ell \in p_x, p_y, p_z} c^{\dagger}_{j,\ell,\uparrow} c_{j,\ell,\uparrow}, \quad (1)$$

where j labels atomic sites (Mn is at $j = 0$), ℓ labels atomic orbitals, and s labels spins. The quantization axis is the spin orientation of the Mn core $3d$ electrons. The LDOS spectra are obtained by calculating the lattice Green's functions with an energy resolution of 10 meV.

Figure 1 shows typical $dI/dV(V)$ curves taken above an acceptor and on the bare InAs surface far from any Mn. The dI/dV signal on Mn shows a sharp peak at

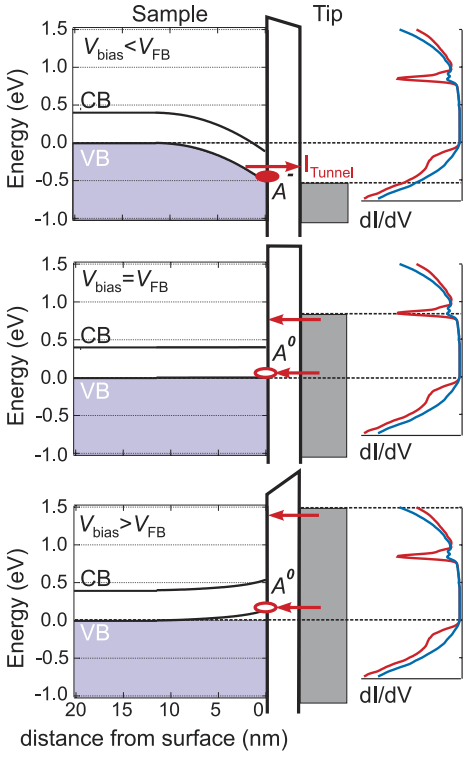

FIG. 1 (color). Left panels: Poisson model of the TIBB at different bias voltages as marked by the Fermi levels of tip and sample (dashed lines). The resulting tunneling paths through the neutral (A^0) or charged (A^-) acceptor are indicated. The tunneling barrier is sketched schematically. Right panels: dI/dV curves measured above a Mn site (red) and on the bare InAs surface (blue). The acceptor state appears as a peak at V_{FB}. ($V_{stab} = 1.5$ V, $I_{stab} = 1$ nA, $V_{mod} = 20$ mV).

$V_{peak} \approx 0.8$ V, i.e., in the region of the bulk CB and not at the VB edge where the acceptor state is located. This apparent discrepancy is due to the tip-induced band bending (TIBB), which shifts the bound hole state across the Fermi level of the sample [6] as sketched in Fig. 1 (left panels). At a certain voltage, the acceptor state crosses the Fermi level resulting in a new tunneling path which appears as a peak in dI/dV. To estimate the TIBB, we use a 1D-Poisson solver neglecting the 3D potential distribution below the tip [20,21]. We use the following parameters: work function for the W tip ($\Phi_{tip} = 4.5$ eV), band gap ($E_g = 0.41$ eV), electron affinity ($E_A = 4.9$ eV), Mn density (10^{19} cm^{-3}), Mn ionization energy ($E_B = 28$ meV), and tip-sample distance (6 Å). The resulting band profiles are plotted in Fig. 1 for different bias voltages. The flat band (FB) condition appears at $eV_{FB} = E_A + E_g - E_B/2 - \Phi_{tip} \approx 0.8$ eV in good agreement with the measured V_{peak}. The position of the peak is slightly different for different acceptors due to the lateral potential fluctuations induced by neighboring charged acceptors and, in turn, can be used to estimate V_{FB} as a function of position. Notice that, for $V < V_{FB}$ ($V > V_{FB}$), the bands bend downwards (upwards) and the Mn acceptor is in the charged state A^- (neutral state A^0) [6].

An STM topograph taken at about V_{FB} is shown in Fig. 2(a). It mainly exhibits the shape of the acceptor states because the tunneling current through the CB states is still relatively small. The different Mn acceptors appear as anisotropic features superimposed on the As sublattice [17]. The depth of the corresponding Mn atoms below the surface is deduced from the topographic height of the observed feature and from the symmetry of the feature with respect to the visible surface As sublattice [6]. It is indicated by numbers (surface layer counted as 0) showing Mn atoms down to ten layers below the surface. The relative orientation of In and As rows deduced from voltage dependent topographs of the bare surface [17] is sketched in Fig. 2(b). A corresponding side view is sketched in Fig. 2(c). Figure 2(d) shows the experimentally observed topographs for Mn atoms at different depths together with the calculated LDOS at the Mn acceptor level in bulk InAs at different distances from the Mn. The topographic height is compared directly with the logarithm of the LDOS [6].

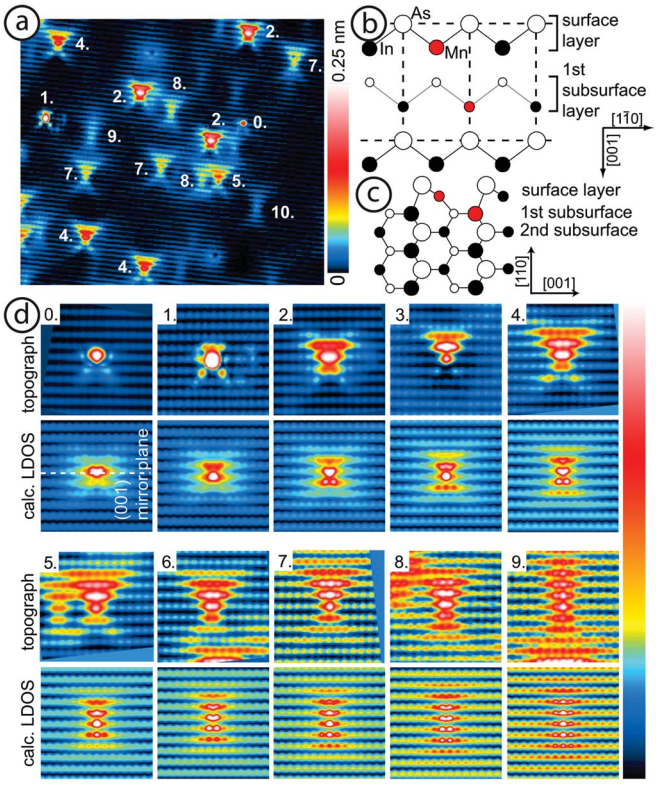

FIG. 2 (color). (a) Topograph at a voltage close to the acceptor level (320 × 365 Å^2, 1.0 V, 0.5 nA). The layer number below the surface where the Mn is located is marked (surface layer counted as 0). (b) Top view model of the (110) surface aligned with the experimental images (surface orientation determined according to [17]); a Mn in the surface and 1st subsurface layer is added; (c) side view according to (b) [17]. (d) Topographs of Mn atoms at different layer depths compared with calculated LDOS at the acceptor energy at different distances from the Mn as marked. The LDOS is plotted on a logarithmic scale with a spatial broadening factor of 2 Å.

The general shapes of the acceptor states are rather similar to the ones observed for Mn in GaAs [6,9]. However, a systematic depth dependence has not been shown for GaAs. Interestingly, the topographic height for the surface Mn appears to be 40% lower than for Mn in the 1st subsurface layer. Although the TBM data largely reproduce the extension and the general shape of the acceptor state, obvious discrepancies are found, in particular, with respect to the (001) mirror plane. For example, the states in the 2nd layer appear brighter above the (001) mirror plane within the STM data but brighter below the (001) mirror plane within the TBM data. The agreement between TBM and STM improves with increasing Mn depth and the shapes are nearly identical for the 8th and 9th layer. This depth corresponds to about half the lateral extension of the acceptor. Therefore, we conclude that the relaxed InAs(110) surface sketched in Fig. 2(c), which is not included in the calculations, has a significant influence on the spatial distribution of the Mn hole state down to about 7 layers. Recently, strain (from an embedded quantum dot) was shown to distort the Mn acceptor wave function in GaAs, lowering the spatial symmetry of the acceptor state [19]. Our result might be important for the coupling in magnetic semiconductor thin films. Notice that asymmetries of shallow-acceptor-related states close to (110) surfaces have been discussed recently for Zn, C and Be impurities [22–25], but without conclusive explanation.

Figure 3(a) shows dI/dV curves on Mn acceptors in different layers. They are recorded with the same tip within a 170×170 Å^2 spectroscopic field consisting of $10^4 dI/dV$ curves [26]. The characteristic peak voltage (A) depends on the spatial position of the Mn, with $V_{\text{peak}} =$ 0.4–0.9 V [cf. peaks of the two 2nd-layer acceptors (1),(2)]. The differences are caused by potential fluctuations due to the random distribution of charged dopants [27]. Close inspection of the upper dI/dV curves reveals at least two additional peaks (B) and (C) above peak (A), with an energetic separation of about 200 mV. These peaks, which appear exclusively around acceptors but never on the bare InAs, thus must be attributed to the Mn. Because of TIBB the undisturbed level spacings to the ground state (A) are a factor of 5 smaller, as can be calculated using the Poisson solver with the corresponding V_{FB}. They are, therefore, 40 mV (B) and 80 mV (C). These splittings are too large to be splittings of the $J = 1$ acceptor ground state by reasonable strains or local electric fields [28]. Similar to the case for Mn in GaAs, our TBM calculations predict that the spin-orbit interaction leads to higher-energy spin states of the bound hole at ~25 meV and ~75 meV above the $J = 1$ ground state. They are shown in Fig. 3(d) and are in good agreement with the experimental data. The excited spin states of neutral Mn acceptors have previously been measured optically [29], but here are seen for the first time for an individual Mn on the local scale.

The influence of the Mn acceptor on the CB and VB can be revealed after subtraction of the dI/dV curve obtained on bare InAs. Corresponding curves above different Mn

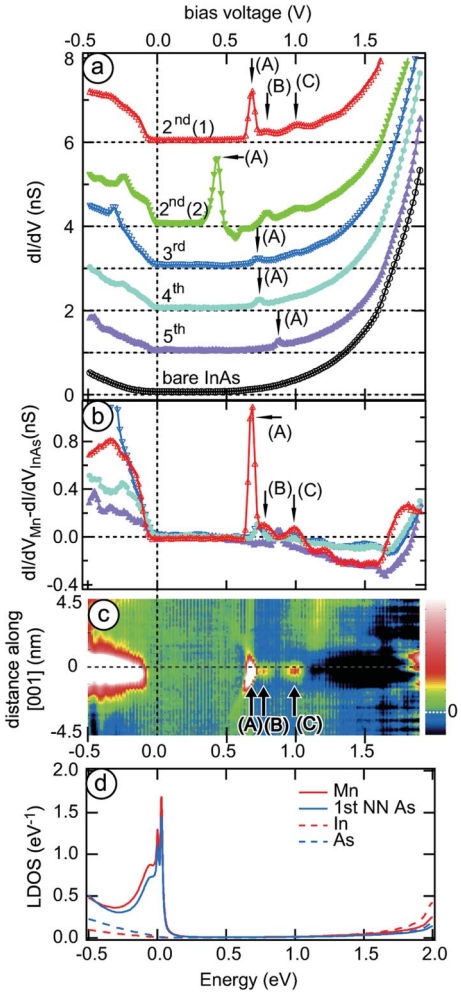

FIG. 3 (color). (a) Spatially resolved dI/dV curves from the bare InAs and on Mn in different subsurface layers as marked [2nd (1) and 2nd (2) denote two different 2nd layer Mn acceptors]. Curves are offset for clarity with dotted zero lines. (b) dI/dV curves on Mn from (a) after subtraction of the InAs curve. (c) Voltage dependent section of the relative differential conductance across a Mn in the 2nd layer. Acceptor-related peaks [(A),(B),(C)] are marked ($V_{\text{stab}} = 2$ V, $I_{\text{stab}} = 2$ nA, $V_{\text{mod}} = 20$ mV). (d) Calculated LDOS at the Mn site, the 1st-nearest-neighbor sites, and at the bare In and As sites.

atoms are shown in Fig. 3(b). Besides the peaks (A),(B),(C), an increase in VB LDOS by up to 400% and a 10% reduction in CB LDOS is observed [30]. The same trend is found in the TBM calculations shown in Fig. 3(d), and is due to the stronger influence of the p-d exchange interaction on the valence band than on the conduction band. Normalized dI/dV curves as shown in Fig. 3(b) are color scaled in Fig. 3(c) up to 4.5 nm away from the Mn. They reveal that the CB suppression and VB enhancement have about the same extension as the acceptor state of 2 nm, and depend only slightly on the energy. A more detailed analysis shows anisotropies to be discussed elsewhere. They are visible in the calculated LDOS in Figs. 4(a)–4(e) as deviations from the circular shape of

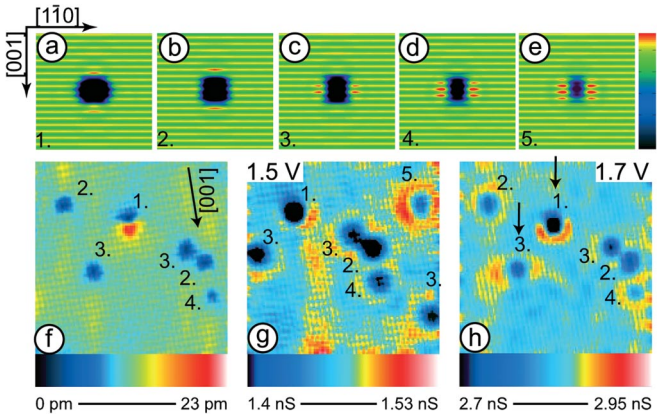

FIG. 4 (color). (a)–(e) 108×108 Å^2 cross-sectional views of the calculated LDOS at 1.4 eV; spatial broadening factor: 5 Å. The distance from the Mn is indicated. (f) 180×180 Å^2 topograph taken at $V_{\mathrm{stab}} = 2$ V. (g),(h) dI/dV maps of an area with the same Mn acceptors as in (f) taken at the indicated voltages.

the dark area around the Mn. More importantly, the extension of the dark area indicating CB suppression is also about 2 nm in the TBM.

Around the depression region of the neutral acceptor, also visible in the dI/dV maps of Figs. 4(g) and 4(h), a ringlike structure appears, which shrinks in diameter with increasing V as expected for the CB scattering states of InAs [31]. The signal for the scattering states is weak in the calculated LDOS, but visible as a slight enhancement of row intensity above and below the dark region in Figs. 4(a) and 4(b) and as a slight enhancement right and left of the dark region in Figs. 4(c)–4(e). The calculated anisotropy of the scattering states depends in detail on the layer as well as on the energy and the strength of the p-d interaction. It is found in a similar fashion in the experimental data, e.g., in Fig. 4(h), as a preferential scattering along $[\bar{1}10]$ for the 3rd layer Mn, but along [001] for the 1st layer Mn (see arrows). However, a more detailed analysis based on additional data is required to extract further information about the p-d interaction beyond the value of V_{pd} we have reported here.

In summary, we have shown that the (001)-mirror asymmetry of the Mn acceptor state in InAs is influenced by the (110) surface down to 7 layers (about the effective Bohr radius), implying that the acceptor-acceptor interaction can be significantly altered by surfaces and interfaces. We also directly observed the higher-spin states of single Mn dopants. An enhancement of VB LDOS and a suppression of CB LDOS was determined in a region of 2 nm around the acceptor, and we found indications of anisotropic scattering of CB states by the acceptor. Most details of the STM results are reproduced by the TBM calculations, stressing the power of this combination for a comprehensive understanding of the local coupling in ferromagnetic semiconductors.

We thank P. M. Koenraad, M. Wenderoth, and S. Loth for helpful discussions and for providing the Poisson solver, O. Albrecht and D. Görlitz for the SQUID measurements, and we acknowledge financial support from SFB508 "Quantum Materials" and Graduiertenkolleg 1286 "Functional Metal-Semiconductor Hybrid Systems" of the DFG.

*Corresponding author.
jwiebe@physnet.uni-hamburg.de
†Present address: Department of Physics, University of New Hampshire, Durham, NH 03824, USA.
‡http://www.nanoscience.de/group_r/

[1] H. Ohno, Science **281**, 951 (1998).
[2] D. D. Awschalom, N. Samarth, and D. Loss, *Semiconductor Spintronics and Quantum Computation* (Springer-Verlag, Berlin, 2002).
[3] A. H. MacDonald, P. Schiffer, and N. Samarth, Nat. Mater. **4**, 195 (2005).
[4] D. D. Awschalom and M. E. Flatté, Nature Phys. **3**, 153 (2007).
[5] R. Wiesendanger, *Scanning Probe Microscopy and Spectroscopy* (Cambridge University Press, Cambridge, England, 1994).
[6] A. M. Yakunin *et al.*, Phys. Rev. Lett. **92**, 216806 (2004).
[7] P. I. Arseev *et al.*, JETP Lett. **77**, 172 (2003).
[8] A. M. Yakunin *et al.*, Phys. Rev. Lett. **95**, 256402 (2005).
[9] D. Kitchen *et al.*, Nature (London) **442**, 436 (2006).
[10] J.-M. Tang and M. E. Flatté, Phys. Rev. Lett. **92**, 047201 (2004).
[11] P. Mahadevan, A. Zunger, and D. D. Sarma, Phys. Rev. Lett. **93**, 177201 (2004).
[12] E. Georgitse, I. Postolaki, V. Smirnov, and P. Untila, Sov. Phys. Semicond. **23**, 469 (1989).
[13] A. Baldereschi and N. O. Lipari, Phys. Rev. B **8**, 2697 (1973).
[14] J. Okabayashi *et al.*, Phys. Rev. B **65**, 161203(R) (2002).
[15] J. Wiebe *et al.*, Rev. Sci. Instrum. **75**, 4871 (2004).
[16] C. Wittneven, R. Dombrowski, S. H. Pan, and R. Wiesendanger, Rev. Sci. Instrum. **68**, 3806 (1997).
[17] J. Klijn *et al.*, Phys. Rev. B **68**, 205327 (2003).
[18] D. J. Chadi, Phys. Rev. B **16**, 790 (1977).
[19] A. M. Yakunin *et al.*, Nat. Mater. **6**, 512 (2007).
[20] G. J. de Raad, D. M. Bruls, P. M. Koenraad, and J. H. Wolter, Phys. Rev. B **66**, 195306 (2002).
[21] R. Dombrowski *et al.*, Phys. Rev. B **59**, 8043 (1999).
[22] R. de Kort *et al.*, Phys. Rev. B **63**, 125336 (2001).
[23] G. Mahieu *et al.*, Phys. Rev. Lett. **94**, 026407 (2005).
[24] S. Loth *et al.*, Phys. Rev. Lett. **96**, 066403 (2006).
[25] S. Loth *et al.*, Jpn. J. Appl. Phys. **45**, 2193 (2006).
[26] Some of the Mn acceptors show negative differential conductivity in a small voltage range above the main peak [cf. 2nd (2) layer Mn], caused by the TIBB as will be discussed in a separate publication.
[27] M. Morgenstern *et al.*, Phys. Rev. Lett. **89**, 136806 (2002).
[28] J.-M. Tang, J. Levy, and M. E. Flatté, Phys. Rev. Lett. **97**, 106803 (2006).
[29] M. Linnarsson *et al.*, Phys. Rev. B **55**, 6938 (1997).
[30] At about 1.75 eV the differential conductivity starts to rise due to the onset of surface states.
[31] C. Wittneven *et al.*, Phys. Rev. Lett. **81**, 5616 (1998).